Ordered structure of $FeGe_2$ formed during solid-phase epitaxy

B. Jenichen,* M. Hanke, S. Gaucher, A. Trampert, and J. Herfort
Paul-Drude-Institut für Festkörperelektronik, Leibniz-Institut im Forschungsverbund Berlin e.V., Hausvogteiplatz 5–7, D-10117 Berlin, Germany

H. Kirmse and B. Haas
Humboldt-Universität zu Berlin, Institut für Physik, Newtonstraße 15, D-12489 Berlin, Germany

E. Willinger and X. Huang
Fritz-Haber-Institut der Max-Planck-Gesellschaft, Faradayweg 4, D-14195 Berlin, Germany

S. C. Erwin
Center for Computational Materials Science, Naval Research Laboratory, Washington, DC 20375, USA
(Dated: July 12, 2019)

Fe_3Si/Ge(Fe,Si)/Fe_3Si thin film stacks were grown by a combination of molecular beam epitaxy and solid phase epitaxy (Ge on Fe_3Si). The stacks were analyzed using electron microscopy, electron diffraction, and synchrotron X-ray diffraction. The Ge(Fe,Si) films crystallize in the well oriented, layered tetragonal structure $FeGe_2$ with space group P4mm . This kind of structure does not exist as a bulk material and is stabilized by solid phase epitaxy of Ge on Fe_3Si. We interpret this as an ordering phenomenon induced by minimization of the elastic energy of the epitaxial film.

arXiv:1907.05189v1 [cond-mat.mtrl-sci] 11 Jul 2019

Ordering phenomena of epitaxial layers have been found in semiconductor mixed crystals as well as in metallic alloys. In general, the ordering has a strong influence on the physical properties of the epitaxial films. In semiconductors (SC), the formation of monolayer superlattices in mixed crystal $Al_xGa_{1-x}As$ epitaxial films grown by metal-organic chemical vapor deposition on (110) or (100) oriented GaAs substrates has been observed.[1] The authors suggested that this long-range ordering is a thermodynamically stable phase at temperatures below about 800 °C. A strain-induced order-disorder transition was found in SiGe epitaxial films grown on Si(001) by molecular beam epitaxy (MBE).[2] This phenomenon later was explained using self-consistent total energy calculations.[3, 4]

For metallic alloys, the amount of collected data is even larger.[5–11] Here, the influence of ordering on material properties like hardness, conductivity, magnetism and corrosion resistance is important. The elastic interaction of the different atoms of the alloys often leads to energetically favored ordered structures. This kind of ordering is influenced by the anisotropy of the crystal lattice.

The structures of the epitaxial Ge and Fe_3Si films on GaAs substrates correspond well to the known structures of their bulk materials.[12–14] However, when the Fe_3Si film is used as a substrate for epitaxial growth of Ge, the influence of the Fe_3Si structure on the growing epitaxial Ge film unexpectedly turns out to be stronger and ordering phenomena occur. These ordering phenomena are induced by the epitaxial growth and were not observed in bulk material up to now. Several methods were applied to achieve perfect semiconducting Ge films on top of ferromagnetic (FM) layers.[15–17] Recently, the method of solid-phase epitaxy (SPE) of Ge was utilized in order to achieve a perfect crystallinity of the film and superior interface quality.[18–20] However, the diffusion of Fe and Si was not entirely prevented during the annealing process. Therefore, the Ge film contained some amount of Fe and Si, leading to a shift of the X-ray diffraction (XRD) peak of the Ge(Fe,Si) film and the formation of a superlattice-like structure inside the Ge(Fe,Si) film. The FM Fe_3Si forms Schottky contacts with the SC Ge and GaAs.[21] A triple layer structure FM-SC-FM is therefore suitable for Schottky barrier tunneling transistors described in [22], similar to tunneling magneto-resistance devices.[23, 24] A spin dependent transport of holes was detected up to room temperature.[20] The aim of the present paper is the investigation of the structure of the Ge(Fe,Si) film.

Fe_3Si/Ge(Fe,Si)/Fe_3Si thin film stacks were grown combining MBE for Fe_3Si on GaAs(001) and SPE for Ge on Fe_3Si.[18] A 36 nm thick Fe_3Si film was grown by MBE on the GaAs buffer layer at a growth rate of 16 nm/h and a temperature of 200 °C in a separate growth chamber dedicated to metal growth. In the same chamber the 4 nm thick Ge film was deposited at 150 °C resulting in a smooth interface but with an amorphous structure. For the SPE of the Ge film the sample was heated at 5 K/min up to a temperature of 240 °C and then annealed for 10 min. The 12 nm thick upper Fe_3Si film was then grown by MBE on top of the crystalline Ge under the same conditions as the lower Fe_3Si film. The growth and annealing conditions of the sample result in a typical structure characteristic for the whole series.[18] After sample preparation transmission electron microscopy (TEM) and XRD (here at an energy of E = 10keV) were used for structural characterization. Experimental details are given in the supplemental material.[25] TEM and XRD simulations

were performed using software packages available.[26–28] In addition, density functional theory (DFT) was employed for the calculation of the lattice parameter and the electronic band structure of the Ge(Fe,Si). DFT in the generalized gradient approximation [29] was applied using the Vienna Ab Initio Simulation Package.[30, 31] The Perdew-Burke-Ernzerhof (PBE) [32] and the Heyd-Scuseria-Ernzerhof (HSE) [33] exchange-correlation functionals, were used for the calculations.

From earlier X-ray results it is clear that the diffusion inside the layer stack has an obvious influence on the formation of the structure of the Ge(Fe,Si) film.[18] Here the diffusion during SPE is more important than the diffusion during the subsequent epitaxial growth of Fe_3Si, because the characteristic structure was observed even without the uppermost Fe_3Si film, and the diffusion during Fe_3Si film growth is known to be low.[34] We obtained the depth dependence of the atomic composition of the different elements by energy dispersive X-ray (EDX) spectroscopy in the scanning TEM (STEM).[25] The Ge(Fe,Si) film consisted of a Ge content of 60±5 at%, an Fe content of 35±5 at% and a Si content of 5±5 at%.[35] Considering in a first approximation the binary phase diagram of Fe–Ge, the phases of FeGe, and $FeGe_2$ could be expected for the given composition range and an annealing temperature of 240 °C during the SPE process.[36] According to such a consideration the $FeGe_2$ should have the tetragonal Al_2Cu structure (I 4/m c m).[37]

Let us consider the formation of our Ge(Fe,Si) thin film structure in more detail. During SPE, an initially amorphous material is annealed on top of a crystalline substrate resulting in a lattice-matched crystalline epitaxial film. In a solid solution inside the growing film, at first sight a random distribution of the elements on the different lattice sites can be expected. However, an ordered distribution of the solute atoms can sometimes lead to a minimum of the free energy F of the system. The distributions of the different elements can be described in the static concentration-wave formalism.[7, 8] A heterogeneity $\Delta(\overrightarrow{r})$ can be written as

$$\Delta(\overrightarrow{r}) \ = \ [n(\overrightarrow{r}) - n_0] \tag{1}$$

where $n(\overrightarrow{r})$ is the occupation probability of a lattice site with a certain type of atom, n_0 is the average concentration of that element, and $\overrightarrow{r}$ is the site-vector of the lattice in the crystalline film. The concentration-wave representation of the heterogeneity $\Delta(\overrightarrow{r})$ is written as follows: If all the positions of the crystal lattice sites are described by one Bravais lattice $\Delta(\overrightarrow{r})$ can be expanded in a Fourier series, i.e. it can be considered as a superposition of static concentration waves:

$$\Delta(\overrightarrow{r}) = \frac{1}{2}\sum_j^{[} Q(\overrightarrow{k_j})exp(i\overrightarrow{k_j}\ \overrightarrow{r}) + Q^*(\overrightarrow{k_j})exp(-i\overrightarrow{k_j}\ \overrightarrow{r})] \tag{2}$$

where $Q(\overrightarrow{k_j})$ is the static concentration wave amplitude and can be treated like a long-range order parameter, and $\overrightarrow{k_j}$ is the nonzero wave-vector of the static concentration wave defined in the first Brillouin zone of the disordered alloy. The index j denotes the wave vectors in the Brillouin zone. The ordering can result in a reduction ΔF of the free energy. Then the uniform solid solution becomes unstable with respect to the heterogeneity (2) with a certain concentration wave vector $\overrightarrow{k} = \overrightarrow{k}_0$. In our epitaxial films we clearly observe such an ordering.

In our experiment, the interface between the underlying Fe_3Si film and an amorphous Ge layer is the starting point of the SPE. The lattice mismatch between Ge and Fe_3Si is $\Delta a/a \ = \ 1.5 \cdot 10^{-4}$. During the deposition of the Ge and the subsequent annealing, Fe and Si atoms diffuse into the Ge film, leading to a small but finite lattice mismatch. This lattice mismatch can be compensated not only by a tetragonal distortion of a disordered Ge(Fe,Si) film, but in addition by an ordering of a substitutional solid solution which can be described as a concentration wave with the wave vector $\overrightarrow{k}_0$. From symmetry considerations, it is clear that the wave vector of the static concentration wave $\overrightarrow{k}_0$ should be perpendicular to the Fe_3Si/Ge(Fe,Si) interface, leaving the properties of the film unchanged along the interface. And indeed, the experimental results obtained earlier by XRD and TEM showed the formation of a superlattice only along one direction, the direction perpendicular to the Fe_3Si/Ge(Fe,Si) interface.[18] A possible choice for the length of the vector is $|\overrightarrow{k}_0| \ = \ 2\pi/c$, where c is the superstructure period observed. At the same time we take c as the lattice parameter of the growing Ge(Fe,Si) lattice perpendicular to the interface, and a as the lattice parameter parallel to the interface. Such a choice of the lattice leads us to the possibility, that the ordering can be described in the frame of the Ge(Fe,Si) lattice itself with a basis of two types of lattice sites described by fractional lattice coordinates: one type occupied mainly by Ge-atoms (or Si-atoms) and the other mainly by Fe-atoms. In this case we can write $(\overrightarrow{k}_0 \cdot \overrightarrow{r}) = 2\pi z$ where z is the coordinate perpendicular to the Fe_3Si/Ge(Fe,Si) interface. The occupation probability $n(z)$ for a certain type of atom is then

$$n(z) = (1/2) \cdot \eta \cdot cos(2\pi z/c) + n_0 \tag{3}$$

where η is the order parameter and n_0 is the average concentration.

A calculation of the change of the free energy ΔF would need more detailed information about the structure of

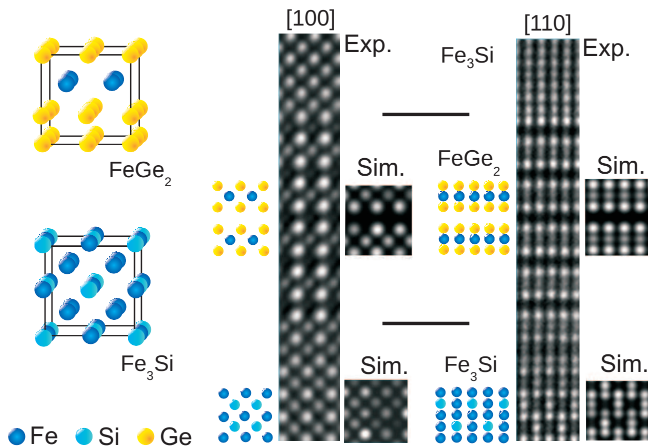

Figure 1. (color online) Comparison of the HAADF experimental cross-section micrographs (larger rectangles, Exp.) with the structural models of $FeGe_2$ P4mm and Fe_3Si shown on the left side as well as the corresponding simulations (small squares, Sim.). The structure of Fe_3Si is well known, whereas the structure of $FeGe_2$ is obtained from the Z-contrast of the present micrographs, taken along the two projections [100] and [110]. The horizontal lines mark the positions of the $FeGe_2/Fe_3Si$ interfaces. They are 1 nm long.

the film. That is why for further investigation of the structure we performed Z-contrast imaging in the STEM. The Z-contrast mode is an incoherent imaging method. In a first approximation presuming constant thickness and neglecting the influence of strain, a high angle annular dark field (HAADF) STEM micrograph exhibits Z-contrast: The intensity diffracted by an atomic column is $I_{HAADF} \sim Z^{1.7...2}$, thus heavier atoms give brighter image contrast.[38] The intensity increases with the number of atoms in a column as well.[39] The STEM micrographs where evaluated using the method of template-matching using the symmetry in the growth plane.[40] Original data is presented in the supplemental material.[25]

In Fig. 1, we can recognize the superstructure in the Ge-rich Ge(Fe,Si) film. The image of the [100] oriented sample shows brighter spots forming a square lattice. These spots are caused by Ge-columns (Z=32). The darker spots, which occur as center of every second square are due to Fe-columns (Z=26). In the image of the [110] oriented sample we see rows of brighter spots and can attribute them to Ge-columns. Between every second pair of bright rows we recognize darker spots and consider them as contrasts due to Fe-columns. In the Fe_3Si film, we recognize the typical Fe-triplets of the image of the [110] oriented sample and the faint spots of the Si-columns between them (Z=14). The image of the [100] oriented sample shows a square lattice of relatively bright spots with darker spots in the centers of the squares. The DO_3 structure of Fe_3Si corresponding to this kind of contrast is known and can serve as a reference. On the basis of the Z-contrast of our HAADF micrographs obtained along the two crystal orientations [100] and [110], we are able to propose a structural model for the Ge(Fe,Si) film: It is the $FeGe_2$ (P4mm) structure shown on the left side of Fig. 1. Four unit cells are depicted for better correspondence with the Fe_3Si lattice. The structural models of Fe_3Si (below, given as a reference) and $FeGe_2$ (above, our proposal) are drawn. The experimental micrographs are compared to the structural models giving an illustration of our proposal of the $FeGe_2$ structure. On the other hand, the well-known structure of the Fe_3Si films is well reproduced, and so we can be sure that we described the $FeGe_2$ structure in a good approximation.

Table I. Experimental lattice parameters (determined by XRD) a of Fe_3Si, and 2a and c of $FeGe_2$ films grown on a GaAs(001) substrate in comparison with unstrained lattice parameters of Fe_3Si and $FeGe_2$ calculated by density functional theory for PBE and HSE functionals.

	EXP	PBE	HSE
a(Fe_3Si)	0.5654 nm	0.561 nm	0.575 nm
2a($FeGe_2$)	0.5654 nm	0.572 nm	0.580 nm
c($FeGe_2$)	0.5517 nm	0.544 nm	0.549 nm

The verification of the proposed $FeGe_2$ structure (see Fig. 1) can be done using computer simulation of HAADF micrographs. We performed the simulations in the frozen phonon approximation using the parameters of the probe-C_s-corrected HR-STEM (JEOL ARM200) operating at 200 kV. Simulations and experimental micrographs shown in Fig. 1 agree well, indicating that a proper structural model was found. The location of the 5 at% Si detected by EDX spectroscopy is still unclear. The Si atoms probably are located on Ge sites. Besides, we found differently ordered regions of the Fe_3Si, the $B2$ order located near the interface and the DO_3 order in depth of the Fe_3Si film.[41]

In Fig. 2 nano-beam diffraction patterns of the thin $FeGe_2$ film from [100] and [110] oriented samples are given. The patterns were fully indexed using the proposed $FeGe_2$ structure model and simulated in kinematical approximation. The results of the simulations given below in red color agree well with the experiments further supporting our structural model.

In Fig. 3, the XRD curve (symmetrical $\omega/2\Theta$-scan, i.e. the 00L crystal truncation rod) together with the simulation of the diffraction curve of the $Fe_3Si/FeGe_2/Fe_3Si$ film stack in the vicinity of the GaAs(002) peak are shown. Here, the simulated diffraction curve agrees with the main features of the experimental diffraction curve, especially the $FeGe_2$ 001 and 003 maxima are visible, and the $FeGe_2$ 002 peak is shifted with respect to GaAs 002. In the supplemental material the XRD reciprocal space map of the non-symmetric 20L crystal truncation rod is shown.[25] All relevant diffraction maxima of the reciprocal space map are positioned on a vertical line per-

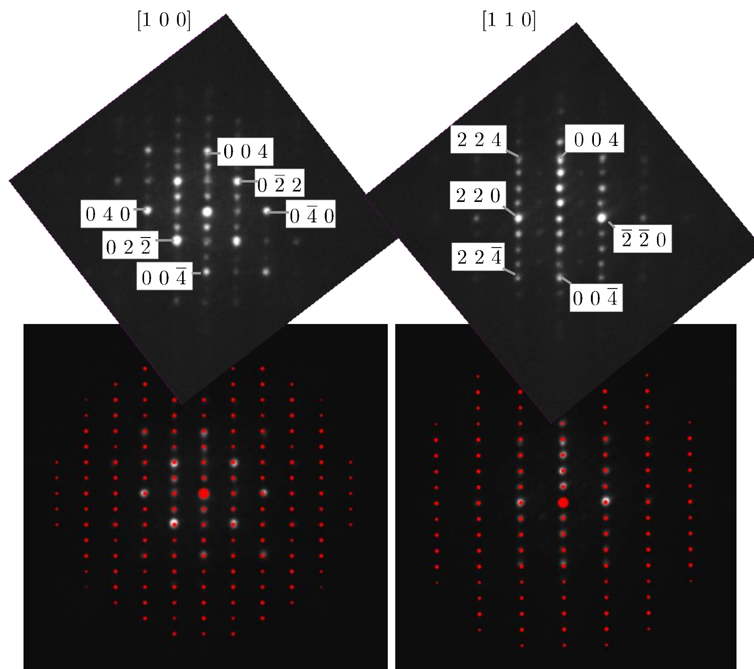

Figure 2. (Color online) Nano-beam diffraction patterns of the thin $FeGe_2$ film from [100] (left) and [110] (right) oriented samples. The comparison of the experimental patterns with the results of the simulations (red) is given below.

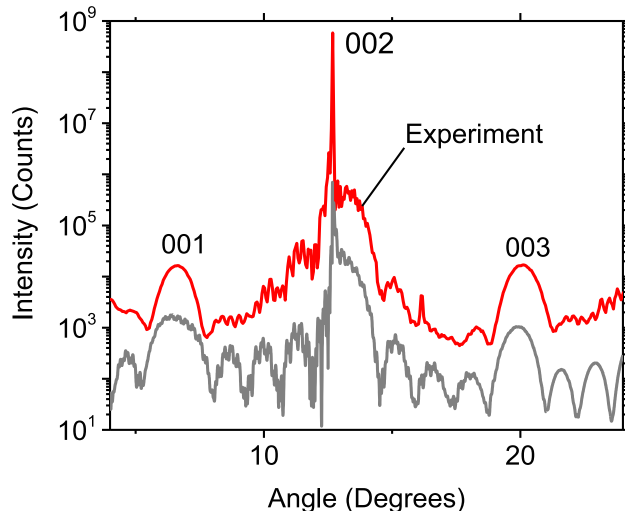

Figure 3. (color online) Comparison of the measured XRD curve and the corresponding simulation (below) near GaAs(002) for the $Fe_3Si/FeGe_2/Fe_3Si$ film stack on GaAs(001), obtained using the structure shown in Figure 1.

pendicular to the sample surface, i.e. the structures are elastically strained and no plastic relaxation occurs.[42] From XRD we deduce the lateral lattice parameter of the epitaxial layer stack a = 0.5654 nm = 2 · 0.2827 nm and the strained vertical lattice parameter of the $FeGe_2$ thin film of c = 0.5517 nm (cf. Table I). A more careful analysis of the STEM HAADF micrographs allowed for determination of the strained lattice plane distances of two types of sublayers in the $FeGe_2$ structure, viz. empty and filled ones. Empty layers and filled layers have distances of c_1 = 0.266 nm and and c_2 = 0.282 nm respectively. Filling with Fe leads to an expansion of the distance of the corresponding layer. This fact points to the possibility of strain compensation between the two sublayers of the $FeGe_2$ lattice as a driving force for the formation of the ordered superlattice-like structure in the epitaxial layer stack.[43] On the other hand, the integral layer thickness c_1+c_2 determined by STEM corresponds well to the strained c-value determined by XRD for the $FeGe_2$ tetragonal lattice as a whole (see above). The theoretical values of the lattice parameters in Table I are given for unstrained lattices. In an epitaxial layer stack additional tetragonal deformation occurs.[35, 44]

Our results show that the ordering can be considered as a systematic arrangement of Fe-atoms and -vacancies in a CsCl-type FeGe lattice, where both atoms and vacancies are found on the Fe-sites, and the number of Fe-atoms is reduced by half in order to obtain the stoichiometry of $FeGe_2$. A random positioning of the Fe-atoms would lead to a cubic lattice. But in our case we have the boundary condition at the $FeGe_2/Fe_3Si$ interface, where the in-plane lattice parameter of $FeGe_2$ is fixed to a value of 0.2827 nm. Let us take two CsCl-type unit cells to describe the $FeGe_2$ lattice as a result of ordering of the Fe atoms and vacancies. Then the diffraction intensity of the fundamental 002 reflection is

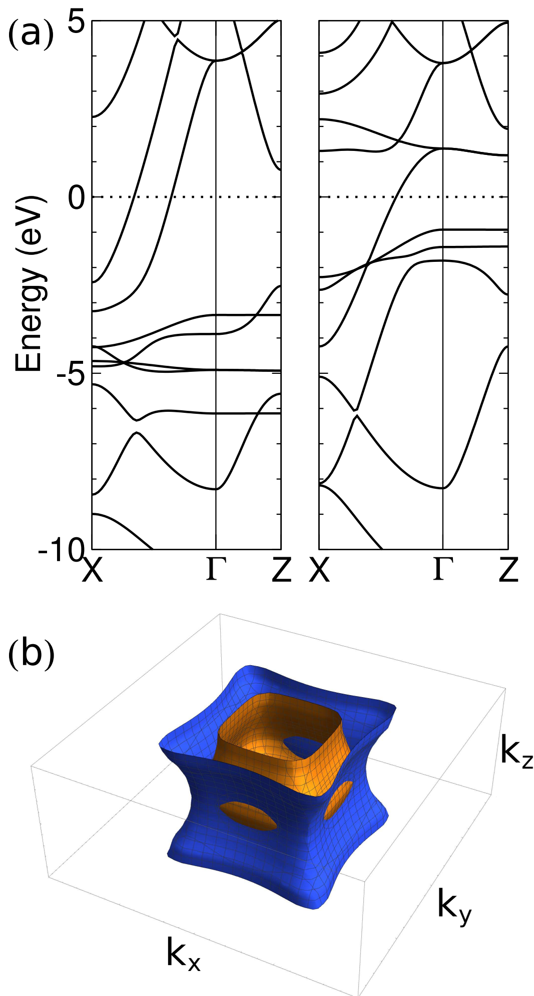

Figure 4. (color online) (a) Band structure of $FeGe_2$ in the P4mm structure calculated using DFT with the HSE screened hybrid functional. Left panel is majority spin; right panel is minority spin. (b) Fermi surfaces for majority (dark, blue) and minority (bright, gold) spins. A second sheet in the majority spin channel is not shown.

proportional to $|f_{Fe} + 2 \cdot f_{Ge}|^2$, where f_{Fe} and f_{Ge} are the atomic form factors of the Fe-atom and the Ge-atom, respectively. The intensity of the 001 superlattice reflection is

$$I(\overrightarrow{k}) \sim |\eta \cdot f_{Fe} - (1-\eta) \cdot f_{Fe}|^2 \quad (4)$$

because all other contributions vanish and only the ordered Fe-atoms give a diffraction signal. From the comparison of the intensities of the layer reflections 001 (superlattice) and 002 (fundamental) we obtain $\eta = (0.805 \pm 0.02)$, i.e the ordering is nearly complete. The film consists of an almost ideal $FeGe_2$ lattice. From the principle of minimum free energy the energy V lost by an atom moving from a disorder position to an order position can be calculated in the Gorsky-Bragg-Williams approximation.[5, 6] This means in our case

$$V = kT \cdot \log[(1+\eta)/(1-\eta)]. \quad (5)$$

For an order parameter $\eta = 0.805$ and our annealing temperature of $T = 513$ K we obtain $V = (0.042 \pm 0.02)$ eV per atom.

Thanks to the ordered structure of the $FeGe_2$ film with the extended Fe-sheets we are expecting outstanding properties of the new material. As a first step, using the structural data of the $FeGe_2$ obtained in the present work, we have calculated by DFT the band structure shown in Fig. 4(a). We can see, that the Fermi surfaces in Fig. 4(b) consist of cylinders along the z-axis, i.e. perpendicular to the Fe-sheets. The electrical properties in the plane of the Fe-sheets probably will differ considerably from those perpendicular to the sheets. $FeGe_2$ belongs to a class of quasi-two-dimensional materials similar to MoS_2.[45] Two-dimensional $FeGe_2$ can now be fabricated with a thickness down to one nanometer, and high–T_C superconductivity seems to be possible in such a structure.[46–49] Thanks to the well ordered Fe-sheets, the concentration-waves can be accompanied by spin-density-waves.

Single crystal Ge-rich films were successfully grown by solid phase epitaxy on $Fe_3Si(001)$. Surprisingly the structure of the films was not the expected diamond structure of Ge, but a well oriented and layered tetragonal $FeGe_2$ P4mm structure. A lattice misfit caused by interdiffusion of Si, Fe, and Ge leads to the formation of a new structure and ordering inside the film. We observe here one of the rare cases, where epitaxy is causing the formation of a distinct crystal structure differing from the equilibrium bulk structure, in particular the strain-induced ordering of the $FeGe_2$ film with a periodicity along the direction perpendicular to the $FeGe_2/Fe_3Si$ interface.

The authors thank Claudia Herrmann for her support during the MBE growth, Doreen Steffen, Margarita Matzek and Sabine Krauß for sample preparation, and Uwe Jahn for critical reading of the manuscript and helpful discussion. This work was supported in part by the Office of Naval Research through the Naval Research Laboratorys Basic Research Program. Some computations were performed at the DoD Major Shared Resource Center at AFRL. We thank the Helmholtz-Zentrum Berlin (HZB) for providing beamtime at the BESSY-beamline U125/2 KMC with the endstation PHARAO.

* bernd.jenichen@pdi-berlin.de

[1] T. S. Kuan, T. F. Kuech, W. I. Wang, and E. L. Wilkie, Phys. Rev. Lett. **54**, 201 (1985).
[2] A. Ourmazd and J. C. Bean, Phys. Rev. Lett. **55**, 765 (1985).

[3] J. L. Martins and A. Zunger, Phys. Rev. Lett. **56**, 1400 (1986).
[4] A. A. Mbaye, L. G. Ferreira, and A. Zunger, Phys. Rev. Lett. **58**, 49 (1987).
[5] W. Gorsky, Z. Phys. **50**, 64 (1928).
[6] E. J. Willliams, Proc. Roy. Soc. A **152**, 231 (1935).
[7] A. G. Khachaturyan, Phys. Stat. Sol. B **60**, 9 (1973).
[8] A. G. Khachaturyan, *Theory of Structural Transformations in Solids* (John Wiley and Sons, Inc., New York, 1983).
[9] A. V. Ruban and I. A. Abrikosov, Rep. Prog. Phys. **71**, 046501 (2008).
[10] I. A. Zhuravlev, J. M. An, and K. D. Belashchenko, Phys. Rev. B **90**, 214108 (2014).
[11] J. S. WrÂ´obel, D. Nguyen-Manh, M. Y. Lavrentiev, M. Muzyk, and S. L. Dudarev, Phys. Rev. B **91**, 024108 (2015).
[12] B. P. Tinkham, B. Jenichen, V. M. Kaganer, R. Shayduk, W. Braun, and K. H. Ploog, J. Cryst. Growth **310**, 3416 (2008).
[13] B. Jenichen, V. M. Kaganer, R. Shayduk, W. Braun, and A. Trampert, Phys. Stat. Sol. A **206**, 1740 (2009).
[14] B. Jenichen, V. M. Kaganer, J. Herfort, D. K. Satapathy, H.-P. Schonherr, W. Braun, and K. H. Ploog, Phys. Rev. B **72**, 075329 (2005).
[15] S. Yamada, K. Tanikawa, M. Miyao, and K. Hamaya, Crystal Growth and Design **12**, 4703 (2012).
[16] B. Jenichen, J. Herfort, U. Jahn, A. Trampert, and H. Riechert, Thin Solid Films **556**, 120 (2014).
[17] M. Kawano, M. Ikawa, K. Arima, S. Yamada, T. Kanashima, and K. Hamaya, J. Appl. Phys. **119**, 045302 (2016).
[18] S. Gaucher, B. Jenichen, J. Kalt, U. Jahn, A. Trampert, and J. Herfort, Appl. Phys. Lett. **110**, 102103 (2017).
[19] S. Sakai, M. Kawano, M. Ikawa, H. Sato, S. Yamada, and K. Hamaya, Semicond. Sci. Technol. **320**, 094005 (2017).
[20] M. Kawano, M. Ikawa, K. Santo, S. Sakai, H. Sato, S. Yamada, and K. Hamaya, Phys. Rev. Materials **1**, 034604 (2017).
[21] K. Hamaya, Y. Baba, G. Takemoto, K. Kasahara, S. Yamada, K. Sawano, and M. Miyao, J. Appl. Phys. **113**, 183713 (2013).
[22] K. Wu, US Patent , 6963121B2 (2005).
[23] S. Yuasa and D. D. Djayaprawira, J. Phys. D: Appl. Phys. **40**, R337 (2007).
[24] M. Oogane and S. Mizukami, Phil. Trans. R. Soc. A **369**, 3037 (2011).
[25] Supplemental material which includes a more detailed description of the TEM and XRD experiments as well as the results of energy dispersive X-ray (EDX) spectroscopy, HAADF original data, and XRD reciprocal space mapping (2018).
[26] P. Stadelmann, *Electron Microscopy Simulation JEMS* (http://www.jems-saas.ch/, Lausanne, 2016).
[27] CrystalMaker, software for interactive crystal/molecular structures: modelling and diffraction by CrystalMaker Software Limited, http://www.crystalmaker.com/ (2017).
[28] S. A. Stepanov, *Collection of x-ray software* (http://sergey.gmca.aps.anl.gov/ , Chicago, 1997).
[29] J. P. Perdew, K. Burke, and M. Ernzerhof, Phys. Rev. Lett. **77**, 3865 (1996).
[30] G. Kresse and J. Furthmuller, Phys. Rev. B **54**, 11169 (1996).
[31] G. Kresse and J. Furthmueller, Comput. Mater. Sci. **6**, 15 (1996).
[32] J. P. Perdew, M. Ernzerhof, and K. Burke, J. Chem. Phys. **105**, 9982 (1996).
[33] J. Heyd, G. E. Scuseria, and M. Ernzerhof, J. Chem. Phys. **118**, 8207 (2003).
[34] J. Herfort, A. Trampert, and K. H. Ploog, Int. J. Mat. Res. **97**, 1026 (2006).
[35] The Si content of 5 atom percent can lead in principle to a lattice contraction of about 0.4 percent. We neglect this in the present work, because we do not know the position of the Si atoms in the lattice. (2018).
[36] R. Jaafar, D. Berling, D. Sébilleau, and G. Garreau, Phys. Rev. B **81**, 155423 (2010).
[37] N. S. Satyamurthy, R. J. Begum, C. S. Somanathan, and M. R. Murthy, Sol. State Com. **3**, 113 (1965).
[38] S. J. Pennycook and D. E. Jesson, Phys. Rev. Lett. **64**, 938 (1990).
[39] S. VanAert, K. J. Batenburg, M. D. Rossel, R. Erni, and G. VanTendeloo, Nature **470**, 374 (2011).
[40] J.-M. Zuo, A. Shah, H. Kim, Y. Meng, W. Gao, and J.-L. RouviÃ©re, Ultramicroscopy **136**, 50 (2014).
[41] M. Hashimoto, A. Trampert, J. Herfort, and K. H. Ploog, J. Vac. Sci. Technol. B **25**, 1453 (2007).
[42] H. Heinke, M. O. Möller, D. Hommel, and G. Landwehr, J. Cryst. Growth **135**, 41 (1994).
[43] DFT yielded the lattice parameters of first a hypothetical primitive Ge lattice: a = 0.268 nm (a = 0.272 nm) and second a hypothetical CsCl-type GeFe lattice: a = 0.288 nm (a = 0.290 nm) correspondingly for HSE(PBE) functional. The halved lattice-parameter a/2 of Fe_3Si of 0.2827 nm lies between those values of the DFT calculations for the hypothetical primitive and the CsCl-type lattices, so that a strain compensation between the two parts of the Ge_2Fe lattice seems possible (2018).
[44] J. Hornstra and W. J. Bartels, J. Cryst. Growth **44**, 513 (1978).
[45] W. Rotjanapittayakul, W. Pijitrojana, T. Archer, S. Sanvito, and J. Prasongkit, Sci. Rep. **8**, 4779 (2018).
[46] G. R. Stewart, Rev. Mod. Phys. **83**, 1589 (2011).
[47] W. Miiller, J. M. Tomczak, J. W. Simonson, G. Smith, G. Kotliar, and M. C. Aronson, J. Phys.: Condens. Matter **27**, 175601 (2015).
[48] J.-F. Ge, Z.-L. Liu, C. Liu, C.-L. Gao, D. Qian, Q.-K. Xue, Y. Liu, and J.-F. Jia, Nature Mat. **14**, 285 (2015).
[49] Y. Zhou, L. Miao, P. Wang, F. F. Zhu, W. X. Jiang, S. W. Jiang, Y. Zhang, B. Lei, X. H. Chen, H. F. Ding, H. Zheng, W. T. Zhang, J. F. Jia, D. Qian, and D. Wu, Phys. Rev Lett. **120**, 097001 (2018).